Pair creation induced by transitions between electronic and positronic bound states

Y. Liu, Q. Z. Lv, Y. T. Li, R. Grobe, and Q. Su

Phys. Rev. A **91**, 052123 — Published 28 May 2015

DOI: 10.1103/PhysRevA.91.052123

Pair creation induced by transitions between electronic and positronic bound states

Y. Liu[(1)], Q.Z. Lv[(2,3)], Y.T. Li[(1)], R. Grobe[(3)] and Q. Su[(1,3)]

(1) Beijing National Laboratory for Condensed Matter Physics, Institute of Physics, Chinese Academy of Sciences, Beijing 100190, China

(2) State Key Laboratory for GeoMechanics and Deep Underground Engineering, China University of Mining and Technology, Beijing 100083, China

(3) Intense Laser Physics Theory Unit and Department of Physics, Illinois State University, Normal, IL 61790-4560, USA

We study the creation process of electron-positron pairs from the quantum electrodynamical vacuum under very strong electric fields by solving the quantum field theoretical Dirac equation on a space-time grid. We investigate the role of bound-bound state mixing in such a process, which can be studied if the external force can be modeled by a combination of a potential barrier and a potential well. By increasing the magnitude of the two potentials, discrete states that originate from the positive and negative energy continua can become quasi-degenerate in the mass gap region (between $-mc^2$ and mc^2). We show that this bound-bound state mixing is quite different from the usual bound-continuum state mixing where the particles are created until the Pauli exclusion principle inhibits this process. In the case of bound-bound mixing the particle number exhibits a characteristic oscillatory behavior that in principle can last forever. All of these findings can be modeled accurately by an effective two-state model.

1. Introduction

One of the most striking predictions of quantum electrodynamics is the possibility to convert light directly into matter. Early works of Sauter [1] and Heisenberg and Euler [2] have suggested that a sufficiently strong external electric field could break down the vacuum and create particle-anti-particle pairs. In 1951 Schwinger [3] used a non-perturbative approach to calculate the required electric field strength required to observe such a process. However, the threshold for the amplitude of the electric field to generate a significant amount of pairs was estimated to be on the order of $\sim 10^{16}$ V/cm, commonly known as the Schwinger field. So far this threshold has not been reached in an experimental setting such that a direct field-matter energy conversion has not been verified in the laboratory yet. Recently several laboratories [4] have begun to develop a new generation of laser systems that could produce sufficiently intense pulses to observe the pair creation process. The intensity for a laser pulse necessary to break down the vacuum is estimated to be on the order of around 10^{29} W/cm^2. Several laboratories are aiming to achieve this critical intensity in the future thus enabling us to observe this fascinating nonlinear quantum electrodynamical process.

Following Schwinger, many theoretical studies [5,6] have continued to calculate the long-time pair creation behavior for spatially inhomogeneous electric fields and several proposals [7-10] have emerged from investigations involving the combination of different static electric, magnetic and time-dependent laser fields in hope to predict the pair creation in a more controllable environment. Many theoretical approaches have been employed to study the pair creation phenomena, such as the proper time method [11-13], WKB approach [14] and various world line instanton techniques [15,16].

Within these theoretical works, there are two challenges that researchers have focused on. One challenge has been to obtain more accurate predictions for realistic laboratory conditions for the onset of pair creation through various spatial and temporal arrangements. The other focus has been to better understand the underlying fundamental mechanisms using large-scale numerical simulations of simplified model systems. In this case the parameters are sometimes chosen beyond experimental feasibility to discover new phenomena. The present work belongs to the latter category where we try to obtain a better understanding of the role of the interactions between electronic and positronic bound states.

In an important work [17,18] it was suggested that electronic bound states that are embedded into the negative energy continuum could be responsible for pair creation in addition to the usual

continuum-continuum state mixing. Recently, several works [19-21] have also suggested that discrete states can act as a transfer channel for population between the positive and negative energy states and thus enhance the pair creation yield.

It is interesting that discrete states have some dynamical relevance even for pair creation scenarios for which the energy spectrum of the underlying Hamiltonian is exclusively continuous. For example, it was recently pointed out that the well-known complex coordinate rotation technique can be applied directly to determine the pair creation rate. Here this technique [22-26] is able to extract truly discrete (and normalizable) states from the continuum. In contrast to the non-relativistic interpretation in terms of finite resonances, in a quantum field theoretical framework of the Dirac multi-particle theory, the lifetime of these states can be associated with pair creation rates.

In this work we study the pair creation process in a novel regime where electronic and positronic bound states in the mass gap are quasi-degenerate. The dynamics of these discrete states turns out to be rather different from the usual bound-free state coupling discussed in the seventies [17]. In order to study the interaction due to these bound states, we require an unusual external field configuration described by a combination of a potential well and a barrier. By varying the height of the potential barrier and well, we can change the energy of the discrete states associated with electronic and positronic energy manifolds and shift them such that they can cross each other. The spatial densities of the created particles suggest that most particles are produced close to the joint of the potential well and the barrier, where the force (proportional to dV/dx) is the maximum.

This paper is organized as follows. In section 2, we describe the physical mechanism for the bound-bound mixing process based on the energy spectrum of the Dirac Hamiltonian. In section 3, we use a one-dimensional potential to investigate the role of discrete electronic and positronic states in the mass gap. This kind of interaction between different discrete electronic and positronic states can be modeled by a simplified two-level system. In Section 4 we study the more complicated case of a time dependent potential, in which we can control the interaction strength between the two bound states. In section 5, more than two bound states are involved and the interaction between different bound states is investigated. In the last section, we provide a brief discussion.

2. The quantum field theoretical approach to pair creation

2.1 The Dirac model system

In order to explore the dynamics of the interaction between discrete states, we use a simplified model described by the Dirac equation for a combination of a potential well with a potential barrier as shown in Fig. 1. The two potentials are separated by a distance F:

$$V(x) = V_0 \, [U(x+F/2) - U(x-F/2)] \qquad (2.1)$$

where each potential is defined as $U(y) = [\, -\tanh[(y-D/2)/W] + \tanh[(y+D/2)/W] \,]/2$ for simplicity. We assume that the potential well and barrier have the same shape and height. This configuration can be characterized by three lengths: W is a measure for the extension of each edge, D is the total width of the potential well or the barrier and F is the length of the region between the barrier and the well.

We can study the number of created electron-positron pairs N(t) as well as the spatial distribution for various parameters. In appendix A we provide the numerical details of how N(t) was computed in quantum field theory from the one-dimensional Dirac equation for the electron-positron field operator.

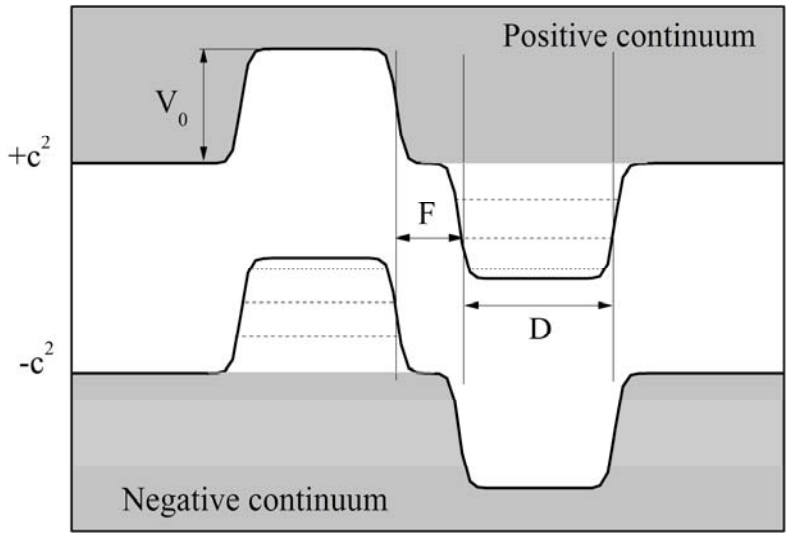

Figure 1 Sketch of the combination of a potential barrier and a potential well. The parameter F is the distance between the two portions of the potential and D is the width of each potential. V_0 ($-V_0$) is the height of the potential barrier (well). The upper (lower) shaded portion indicates the positive (negative) continuum. The dashed lines show the bound states in the potential well and barrier. Here the dotted lines indicate the first bound states from the negative continuum and positive continuum that can have the same energy.

Before analyzing the simulation results in more detail, let us first describe the resonance mechanism of two bound states in more detail. The field-free positive ($E>c^2$) and negative continuum ($E<-c^2$) states do not overlap in the absence of forces. If a potential well (barrier) is turned on, unfilled (filled) bound states emerge from the positive (negative) continuum. We associate the bound states of the potential well (barrier) with electronic (positronic) states that are initially unoccupied (occupied) consistent with the Dirac sea representing the vacuum state.

By increasing the height V_0 of the potential, the bound states emerging from the positive and negative continua come closer to each other and can even cross if the potentials are sufficiently large. This process can be associated with the creation of an electron-positron pair. The created electron is then trapped in the potential well, while the positron is captured by the barrier.

To be more quantitative, we show in Figure 2 the energy spectrum of the total Dirac Hamiltonian as a function of the height V_0. Due to the presence of the bound states, the spectrum in the energy gap forms a "net" like structure in the shape of arrays of quadrangles. The three vertical lines indicate the first four avoided crossing points. In this work we focus our attention to the properties of the four crossing points in the first quadrangle. When the potential strength V_0 is $1.102c^2$ (labeled 1) there are a total of eight bound states emerged from the positive and negative energy continua. The first positive and negative bound states approach each other in the middle of the mass gap region, close to $E=0\ c^2$, but keep a minimum separation of $0.00414c^2$ characteristic of an avoided crossing. For $V_0=1.235c^2$, there are two avoided crossings (labeled 2 and 3) $0.129c^2$ ($0.126c^2$ and $0.133c^2$) and $-0.129c^2$ ($-0.126c^2$ and $-0.133c^2$). The minimum separations are $0.006c^2$ in both cases. Moreover, when $V_0=1.375c^2$ (labeled 4), the second set of discrete states (first excited states) from the two continua show an avoided crossing with the two energies $0.0056c^2$ and $-0.0056c^2$.

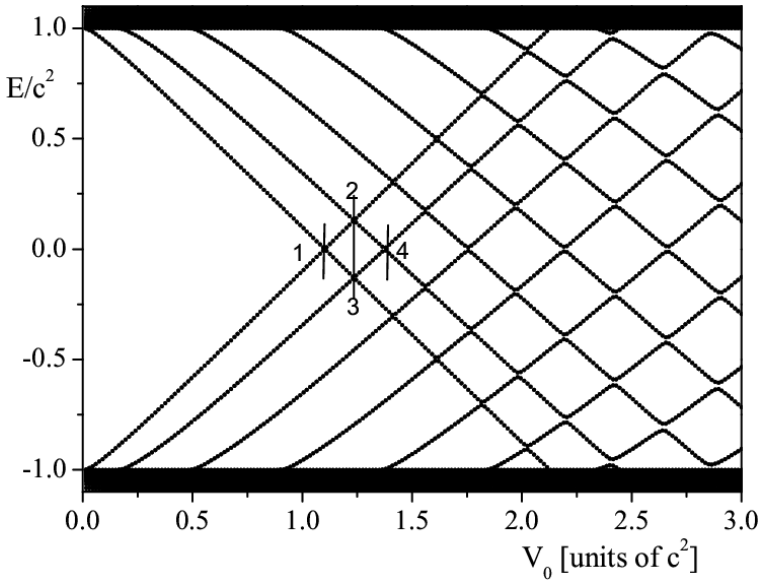

Figure 2 The energy spectrum of the total Dirac Hamiltonian as a function of the height V_0 of the potential displayed in Figure 1. The four vertical lines mark the first four avoided crossing points. [The parameters are W=0.3/c, D=6/c and F=2.4/c]

The total number of the avoid crossings in the energy gap (from $-c^2$ to $+c^2$) for D=6/c alternates between five and six for large values of V_0. However, if we increase the potential well (barrier) width D, the maximum number of crossing points increases, and when D approaches infinity, the number of crossing points is sufficiently large such that the bound states in the gap become very dense leading to an overlap of effectively positive and negative quasi-continua. The energy difference at each crossing point decreases with the increasing of F, which is related to the coupling strength between the two states as we will discuss in more detail below.

2.2 The model based on the two-level approximation

In this section we motivate the two-state approximation. It is important to remember that in this study (and in almost any other works in the literature [27]) the definition of the created particles is based on the projection on the force-free (and not the actual) energy eigenstates, denoted in Eq. (A.3) as $|p\rangle$ and $|n\rangle$. Also, in this work we have assumed that in each simulation the external force is absent initially, such that the vacuum state is described by the sum of all occupied states $|n\rangle$.

If the external force is then turned on abruptly (or over a sufficiently short time period), then the total overlap of the electronic manifold of the energy eigenstates of the coupled system with all states $|n\rangle$ determines the number of created particle pairs. For example, the usual relativistic

hydrogen atom is a pure one-electron system, but nevertheless its ground state $|1s\rangle$ has a non-vanishing overlap with the force-free states $\langle n|1s\rangle \neq 0$. This means that if a proton were suddenly inserted into the universe, the resulting boost to the vacuum would create electron-positron pairs, where part of the electron could occupy the ground state (in this newly formed hydrogen atom) with a probability that is given by $\Sigma_n |\langle 1s|\square\rangle|^2$. Equivalently, if the proton were removed instantly from a hydrogen atom in its ground state, positrons with an average number of $\Sigma_n |\langle 1s|\square\rangle|^2$ would occur. It is therefore important to study the overlap of the states $|\square\rangle$ with the true energy eigenstates of our specific system, defined by the Dirac Hamiltonian in Eq. (A.1).

In Figure 3 we have graphed this total overlap $O_n(E) \equiv \Sigma_n |\langle E|\square\rangle|^2$ for the positronic ground state with all force-free states of the negative energy as a function of the ground state energy, which depends directly on V_0. Its should be obvious that the corresponding overlap with the states $|p\rangle$ is simply given by $O_p(E) \equiv \Sigma_p |\langle E|p\rangle|^2 = 1 - O_n(E)$.

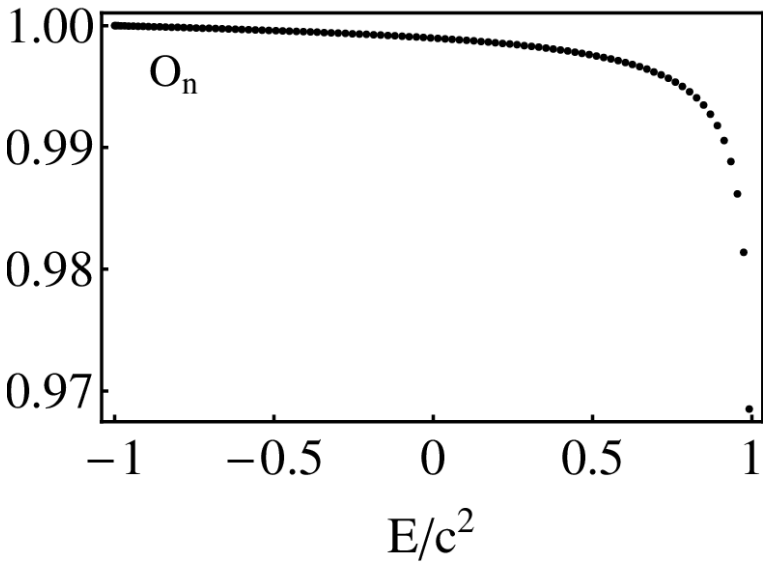

Figure 3 The overlap of the positronic bound state with all force-free states of the negative energy as a function of the energy of this state, $\Sigma_n |\langle E|n\rangle|^2$. V_0 was increased from 0 to $2.2c^2$.
[other parameters are W=0.3/c, D=6/c, only the well portion of the potential was used corresponding to $F \rightarrow \infty$].

The data suggest that the weight factors $\{\sqrt{O_p}, \sqrt{O_n}\}$ for this particular state change from {0,1} for $E= -c^2$ (corresponding to $V_0=0$) to {0.1764, 0.9843} for $E=0.99c^2$ (corresponding to $V_0=2.2c^2$).

Similarly (not shown), the corresponding electronic ground state would change from {1,0} for $E=c^2$ to {0.9838, 0.1792} for $E=-0.99c^2$. In other words, while the energy of these states changes significantly by $2c^2$, the weight factors did not change too much and stayed rather robustly the same close to 1.

The data were obtained for the potential well. In the dynamical region close to the avoided crossing of an electronic and positronic bound state the pair creation dynamics is largely governed by only two eigenstates. In the absence of any coupling (corresponding to an infinite spacing between the well and barrier, $F\rightarrow\infty$) we loosely label the electronic states as {1,0} and positronic state as {0,1} for all V_0 as suggested by the data in Figure 3. The energy of these states as a function of V_0 could be modeled by the matrix

$$H = [\{c^2-v(V_0), 0\},\{ 0, -c^2+v(V_0)\}] \qquad (2.2)$$

where we defined the scaled potential height as $v(V_0) \equiv V_0/1.102$ for the first avoided crossing. The scaling of the height was introduced such that (for $F\rightarrow\infty$) , the two eigenvalues of H, $c^2-V_0/1.102$ and $-c^2 + V_0/1.102$, can follow a similar path as a function of V_0 as the exact electronic and positronic bound states shown in Fig. 2. For example, for $V_0 =1.102c^2$ we would have a perfect energy degeneracy. Here the eigen vectors remain precisely {1,0} and {0,1}, independent of V_0.

To include the effect of a non-infinite spacing F, the dynamical evolution of the two discrete states can be approximately described in this basis by an effective two-state Hamiltonian given by the 2×2 matrix

$$H = [\{c^2-v(V_0), \lambda(F)\},\{ \lambda(F), -c^2+v(V_0)\}] \qquad (2.3)$$

To find the best match for our numerical parameters, we have to define an effective coupling $\lambda(F)$. The coupling $\lambda(F)$ between the two states has to decrease as the spacing F increases. In atomic units any energy is inversely proportional to the square of a length. In order to model an effective coupling interaction energy we chose $\lambda(F) =0.02765\ c^2 \exp(-F/0.898)$ for the first avoided crossing. This particular pre-factor was chosen phenomenologically based on the minimum energy spacing at the avoided crossing.

In the sections 3, 4 and 5 below, we will describe several scenarios where the potential height $V_0(t)$ and the spacing F(t) between the two potentials vary in time. In the two-state model we can approximate this by permitting the parameters v and λ to become time dependent. The general time evolution from an initial state $|\Psi(t=0)\rangle = \{0,1\}$ to the state $|\Psi(t)\rangle = C_1(t)\ \{1,0\} + C_2(t)\ \{0,1\}$ can be obtained easily from this model by solving the coupled equations for a given v(t) and λ(t).

$$i\, dC_1(t)/dt \;=\; [c^2\text{-}v(t)]\, C_1(t) \;+\; \lambda(t)\, C_2(t) \qquad (2.4a)$$

$$i\, dC_2(t)/dt \;=\; [-c^2\text{+}v(t)]\, C_2(t) \;+\; \lambda(t)\, C_1(t) \qquad (2.4b)$$

In this model the number of created particle pairs trapped in the bound states is simply associated with the population of the state labeled {1,0}, as the overlap with the positive free states was denoted by the upper component, $N(t) = |C_1(t)|^2$ with N(t=0) = 0.

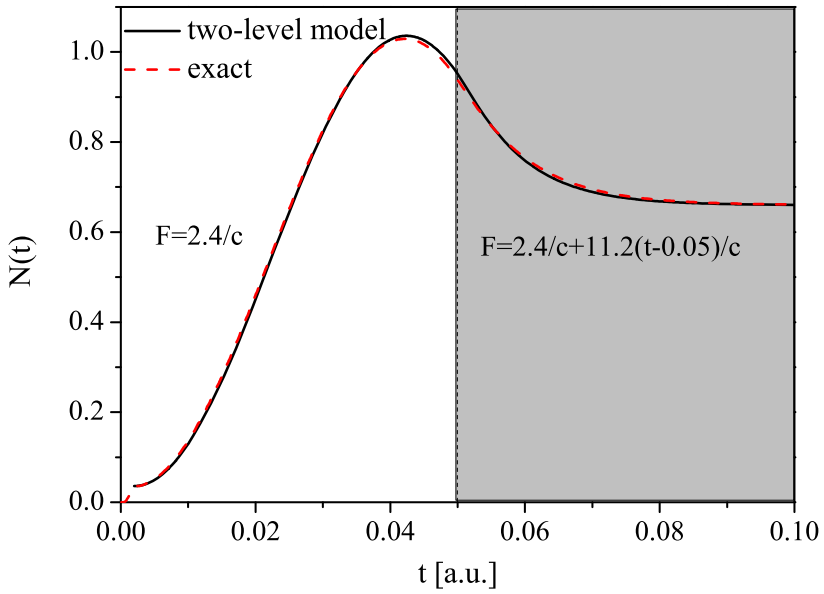

Figure 4 (Color online) The number of the created electrons N(t) as function of time. The red curve is the exact particle number and the black curve is the prediction from the solution of the two-level approximation. Before t=0.05, F=2.4/c, and in the interval 0.05<t< 0.1, F is increased linearly from 2.4/c to 8/c [other parameters are W=0.3/c, D=6/c].

In Figure 4 we have tested the validity of the two-level approximation for a system in which first the potential height was varied (for t≤0.002) and then the distance between the two potentials was increased (for 0.05≤t≤0.1). More specifically, the amplitude V_0 was turned on according to $\sin^2(\pi t/0.004)$, while F was increased linearly from 2.4/c to 8/c with F=2.4/c +11.2(t–0.05)/c. This

good agreement of the exact numerical curve and the predictions of this model for the overall behavior of N(t) establishes the validity of the phenomenological two-level model for a general condition.

3. The pair creation around the first crossing point

As discussed in Figure 2, the first crossing point occurs at $V_0=1.102c^2$ close to the energy $E=0c^2$. As this energy is different than that of any other states, it seems reasonable to assume that the pair creation process close to this resonance can be modeled by only two states. While it is numerically rather straightforward to solve the two equations numerically, one can obtain useful insight into the dynamics for more special situations where neither the amplitude V_0 (modeled above by v) nor the spacing F (modeled by λ) vary too rapidly in time. For example, in the adiabatic case, the instantaneous energy eigenvectors of the effective two-state Hamiltonian of Eq. (2.3) can play a significant role. We show in Appendix B that if the force is turned on rather abruptly the number of created electron-positron pairs is given by the oscillatory function

$$N(t) = \left|\exp(-i\, E_{pos}\, t)\, V_{pos2}V_{pos1} + \exp(-i\, E_{neg}\, t)\, V_{neg2}V_{neg1}\right| \qquad (3.1)$$

where $\{V_{pos1},V_{pos2}\}$ and $\{V_{neg1},V_{neg2}\}$ are the components of the instantaneous energy states with energies E_{pos} and E_{neg} .

3.1 The particle yield N(t)

The inset of Figure 5 is the zoomed-in view of the energy spectrum of the total Hamiltonian as a function of V_0 close to the first crossing point at $V_0=1.102c^2$, where the two states take the energies $\pm 0.00207c^2$. The five vertical lines indicate $V_0 = (1.095, 1.099, 1.102, 1.105 \text{ and } 1.109)\, c^2$, with the corresponding energy differences $\Delta E = (0.0140, 0.0070, 0.0040, 0.0073 \text{ and } 0.0144)\, c^2$. The solid curves in the inset are the energy spectrum obtained from the simple two-level model by diagonalizing the effective 2-state Hamiltonian of Eq. (2.3). Here we choose for the energy $v(V_0) = V_0/1.102$ and for the coupling between the two states $\lambda(F) = 0.02765c^2 \exp(-F/0.898)$. We can see that the match is superb especially near the avoided crossing. When V_0 is increased or decreased from $1.102c^2$, the energy difference between the two discrete states ΔE grows.

The solid curves in the main Figure 5 are the corresponding time dependent numbers of created particles N(t) associated with five potential heights. These heights are chosen symmetric around $V_0=1.102c^2$ and the data for N(t) show that the corresponding pair creation yields are also roughly symmetric around $V_0=1.102c^2$.

We note that each graph is characterized by three different temporal regimes. At very early times ($t_s<0.002$) when the field was turned on [with an amplitude $\sin^2(\pi t/0.004)$] the number of pairs grows smoothly in time. Had we chosen an even more abrupt turn on, N(t) would be more oscillatory, reflecting the high frequencies that are unavoidable for this rapid turn on. In the next time regime the electrons (positrons) are created in the region between the two potentials and move away to the outside edges of the well (barrier). Before they reach the other edges, the creation behavior can be characterized by a universal linear growth in time $N(t)\sim r(V_0,F)\, t$, where the corresponding rate $r(V_0,F)$ depends on the height V_0 (assumed to be the same for the potential barrier and the potential well) and the spacing F. In this regime, our field configuration can be viewed as two subcritical potentials arranged side by side. Similar configurations have been studied by Jiang et al. [19]. In the third regime, the pair creation yields for the five potentials begin to differ and exhibit an oscillatory behavior with a distinct period and amplitude for each graph. For example for $V_0=1.095c^2$ there are two full cycles. The yield N(t) grows and at t=0.0138 a.u. it reaches a maximum of 0.117. At time t=0.0254 a.u., N(t) takes the minimum value 0.034 leading to an overall period of T=0.0232 a.u.. For the other four heights [$V_0=(1.099, 1.102, 1.105$ and $1.109)c^2$] the periods are 0.0474, 0.0800, 0.0448 and 0.0223, respectively. On the other hand, the corresponding highest yields are 0.117, 0.381, 1.027, 0.354 and 0.12.

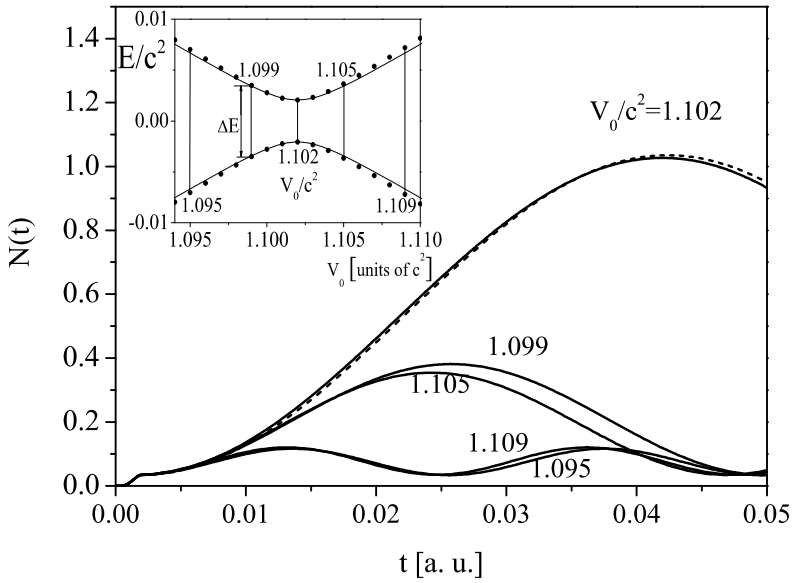

Figure 5 The number of the created electrons as a function of time for the potential heights V_0=1.095c^2, 1.099c^2, 1.102c^2, 1.105c^2 and 1.109c^2 (vertical lines in the inset). The dashed line [Eq. (3.2)] for V_0=1.102c^2 is the prediction of the two-state model. The inset (dots) indicates the energy spectrum of the total Hamiltonian as a function of height V_0 of the potential shown in Figure 1 and the two solid curves are due to the two-level theory. [Parameters are W=0.3/c and D=6/c, F=2.4/c.]

We therefore have the largest yield for V_0 = 1.102c^2, which also leads to the longest period. In order to explain this phenomenon, we employ an effective two-level model. The dashed curve in the Figure is the result from the two-level model calculation. For V_0=1.102c^2, the agreement between the exact data and the prediction due to the simple two-level model is quite remarkable and suggests that indeed only the two discrete states are responsible for the total pair creation yield. In the two-level system, the period of the oscillation T can be directly determined from the difference of the two energy levels ΔE, as T =2π/ΔE. In our simulation, the period for V_0=1.102c^2 turned out to be T =0.0800 a.u., while the theoretical value from the two level is 0.0836 a.u.. The difference is only 4.5%.

Since only a single electronic and a positronic bound state are involved in the process, we would expect that the pair creation yield should become at most equal to 1. However, from Figure 5, we see that the height of potential V_0 has a strong influence on the actual yield N_{max}.

In Figure 6 we have therefore monitored the largest yield as a function of V_0 for two different separations F. Only when the system is closest to the avoided crossing point, the peak value of the curve is 1. According to the two-level model [discussed in Appendix B], the maximum particle

number can be obtained as:

$$N_{max} = V_{pos1}^{\ 2}\, V_{pos2}^{\ 2} + V_{neg1}^{\ 2}\, V_{neg2}^{\ 2} + 2\,|V_{pos1}\, V_{pos2}\, V_{neg1}\, V_{neg2}| \qquad (3.2)$$

Where once again $\{V_{pos1}, V_{pos2}\}$ and $\{V_{neg1}, V_{neg2}\}$ are the components of the instantaneous energy eigenstates, which are functions of V_0 and F. The match between the data from the exact simulations and the theoretical approximations for F=2/c and 4/c is again quite remarkable.

For F=2/c, the maximum yield at $V_0 = 1.102c^2$ is 1.055. The small amount of excess yield (0.055) is due to the turn-on of the field not being sufficiently slow. When V_0 increases or decreases around the crossing point, the yield is reduced symmetrically. This is the same result as in Figure 5. When the system is far away from the avoided crossing, the energy difference between the two states becomes large and the transition from the lower level to the upper level becomes difficult. This can also be seen from the two-level model. The instantaneous upper eigenstate of the two-level Hamiltonian is {–0.157, 0.988} for $V_0=1.095c^2$, while the corresponding state at the avoided crossing is {0.707, –0.707}.

The second factor that influences the peak value of the particle number N_{max} is the distance F between the potential well and barrier. In Figure 6 we also compare $N_{max}(V_0)$ for two different F. The resonance profile for F=4/c is much narrower than the one for F=2/c. The full width at half maximum of the peak for F=2/c is $0.0071c^2$, while for F=4/c it is only $0.0010c^2$.

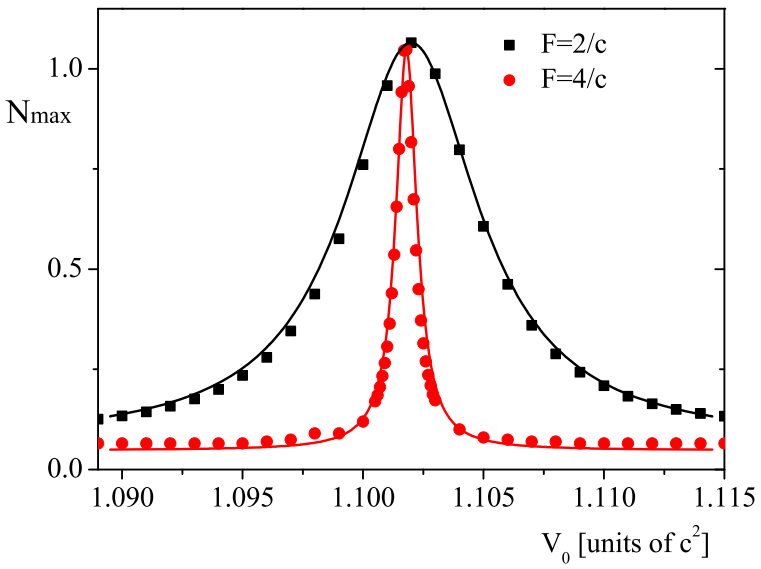

Figure 6 (Color online) The largest yield N_{max} as a function of the height V_0 for F=2/c (black squares) and 4/c (red circles). For comparison, the solid lines (black and red) are due to the two-level model Eq. (3.4). [Parameters are W=0.3/c and D=6/c]

3.2 The spatial distributions of the electrons and the positrons

The yields N(t) in Figure 5 suggest that the electrons are created and then subsequently annihilated again. In order to study this periodic phenomenon from a spatially resolved perspective we calculate the spatial distribution of the created electrons and positrons in Figure 7. As a reference we also show the potential V(x) at the bottom of each panel.

In the figure, we compare the densities with those based on the two-level model. Here use the true eigenstates, $\chi_+(x) \equiv \{P_1(x), P_2(x)\}$ and $\chi_-(x) \equiv \{N_1(x), N_2(x)\}$, which are calculated by diagonalization of the full Hamiltonian in Eq. (B.1) in a spatial basis. As a result, the state is $\Psi(x,t) = \exp(-i\, E_{pos} t)\, V_{pos2}\, \chi_+(x) + \exp(-i\, E_{neg} t)\, V_{neg2}\, \chi_-(x)$. The coefficients V_{pos2} and V_{neg2} are determined directly from the two-level model. The effective spatial density for electrons and positrons is then given by

$$\rho_{electron}(x,t) \equiv |\langle\{1,0\}|\Psi\rangle|^2 = |\exp(-i\, E_{pos} t)\, V_{pos2}\, P_1(x) + \exp(-i\, E_{neg} t)\, V_{neg2}\, N_1(x)|^2 \quad (3.3a)$$

$$\rho_{positron}(x,t) \equiv |\langle\{0,1\}|\Psi\rangle|^2 = |\exp(-i\, E_{pos} t)\, V_{pos1}\, P_2(x) + \exp(-i\, E_{neg} t)\, V_{neg1}\, N_2(x)|^2 \quad (3.3b)$$

In the Figure, the solid curves are the numerical results and the dashed lines are obtained from Eq. (3.3). From the first two panels, we can see that the particles are created at short times near the potential well/barrier edges, where electric field is the strongest. Consequently, they move to the middle of the potential well/barrier. Note that both particles are present in the potential well and barrier indicating it takes time for charges to develop. At later times the electrons (positrons) are located in the potential well (barrier) and their population increases and decreases in a periodic fashion.

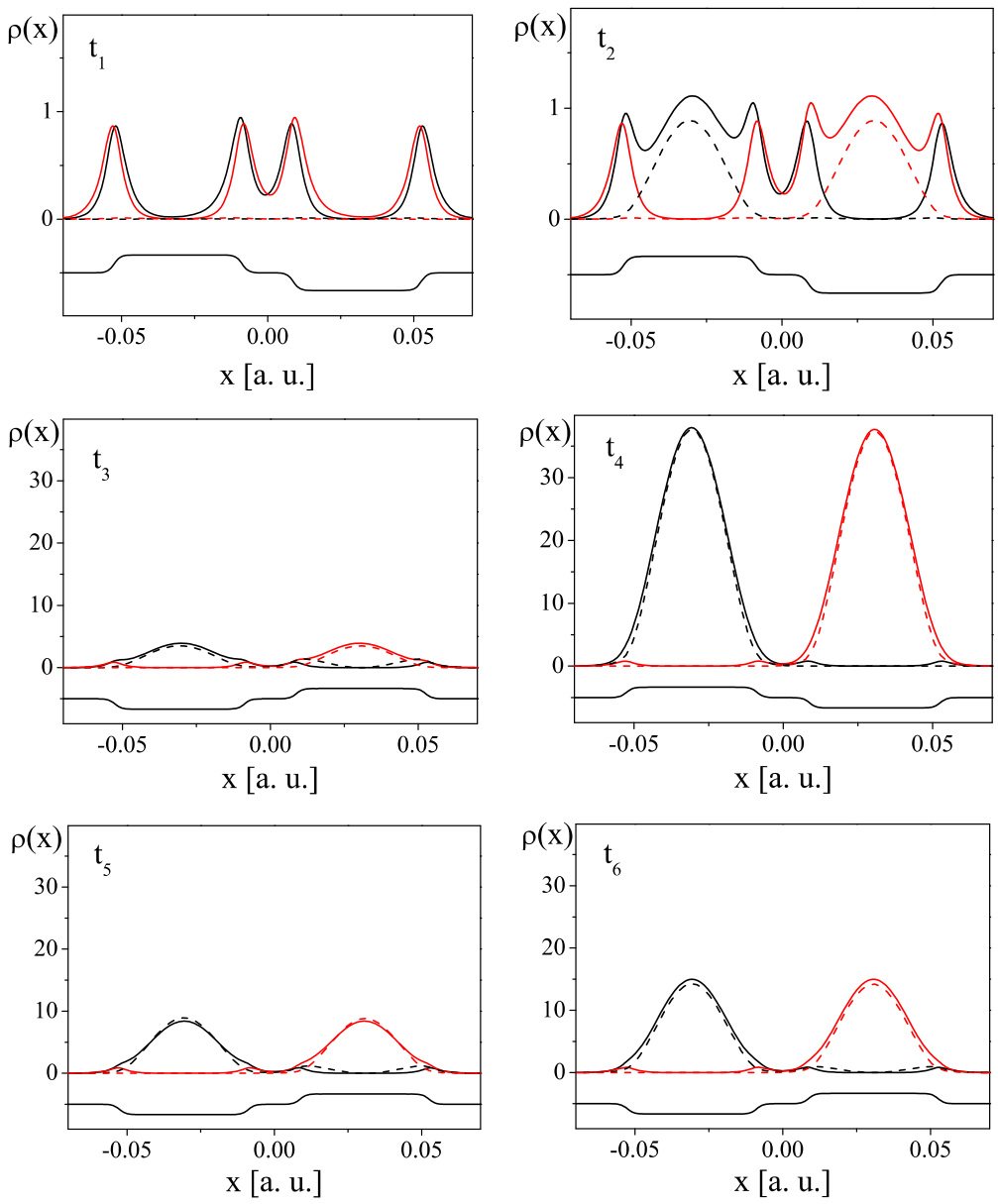

Figure 7 (Color online) Snapshots of the electron (red curves) and positron (black curves) spatial densities at times t_i = 0.002, 0.006, and 0.01a.u. (i=1,2,3) and t_i = 0.04, 0.07, and 0.10 a.u.(i=4,5,6). The dashed curves are due to the two-level theory. [All parameters are the same as in Fig. 5, N_x=1024, L=0.5a.u., V_0=1.102c^2, D=6/c, F=2.4/c and W=0.3/c]

At t=0.01, the electron density (red curve) has four very small peaks, two of which are at the edge of the potential well. Those can be viewed as the ghost states [20] as they do not change with time unless the external field changes. The area under the main peak in the well is 0.1200, which is in close agreement with the particle number (0.1365) shown in Fig. 5. When t=0.04 a.u., the peak grows and its area is 1.007, which is again in agreement with data (1.0208) of Fig. 5. After this time,

the peak becomes small again. The area at t=0.07a.u. is 0.2370. This represents the annihilation of the particles. However, when t=0.10 a.u., the area again grows to 0.4073. We also note that our simplified two-level model describes all of these data again rather well.

The created positrons (black curves), which are captured in the potential barrier, show a similar behavior as the electrons. This synchronous but mirror symmetric behavior between the electrons and positrons is expected. As the potential does not change in time the population of the energy eigenstates is constant in time. The population of the created electrons, however, depends on the upper component of the superposition state of both eigenstates and therefore can change in time. At the avoided crossing both bound states are equally and perfectly excited from the Dirac sea. But as each bound state represents only 50% of an electron (and positron) the maximum number of created electrons can be at most equal to 1.

We note that the spatial densities in each potential grow in synch. In other words, the population does not tunnel periodically back and forth between both potentials as a single particle wave packet would between two nearly degenerate bound states. This pair creation process at the avoided crossing point is also analogous to the bound-continuum degeneracy situation. The only difference is that in the bound-bound mixing case, the potential must have a special height in order to induce the resonance while in the bound-continuum situation the potential just needs to be supercritical.

4. Control of the pair creation yield by time-depending force fields

We have seen that for a rather sudden turn on of the force the number of created particles can oscillate periodically due to the interference between both bound states. We also observed that the period and amplitude of the oscillations are rather sensitive to the potential height and the separation between the potential barrier and well. In the following we demonstrate how one can control the total yield by varying F and V_0.

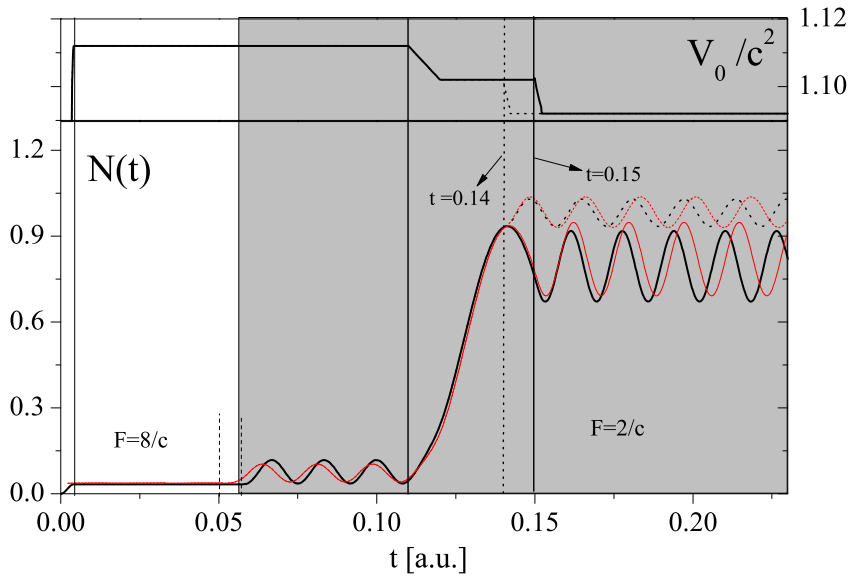

Figure 8 (Color online) The number of created pairs as a function of time for a time-varying force. The top panel shows how the height V_0 changes as a function of time. The three vertical lines indicate V_0=1.112 c^2, 1.102 c^2 and 1.092c^2. The red curves are obtained from Eq. (3.2). F takes the value of 8/c in the white region and then becomes 2/c in the grey region. [Parameters are T_{max}=0.23, D=6/c, W=0.3/c].

In Figure 8 we show N(t) for a time-dependent potential. During a short initial time interval ($t \leq 0.002$) the potential was turned on to $V_0 = 1.112c^2$ with an amplitude function $\sin^2(\pi t/0.004)$ while the well and the barrier are basically infinitely apart (F=8/c). For $V_0 = 1.112c^2$ the bound state originating from the negative continuum has a higher energy than the one from the positive continuum, and the yield approaches quickly the low value of 0.024, which is basically due to the unavoidably high frequency components of the turn-on amplitude.

In the second domain, $0.002 \leq t \leq 0.05$, the height $V_0 = 1.112c^2$ and F=8/c are kept constant and the yield does not change. The constant N(t) can be either associated with the fact that for ($F=\infty$) only a single bound state has a significant overlap with the Dirac sea or (in case of equal excitation) both states are precisely energy degenerate and therefore evolve with the same phase.

In the third domain ($0.05 \leq t \leq 0.06$), we decreased the distance F between the potential well and barrier from the initial value 8/c to 2/c, according to function 8/c-600(t-0.05)/c. In the forth domain ($0.06 \leq t \leq 0.11$), we kept all parameters constant to give the system sufficient time to react to the earlier changes. Due to the coupling between the two bound states N(t) oscillates with a period of T=0.017, which is in nice agreement with the period (0.0176) calculated from $T=2\pi/\Delta E$ (where

$\Delta E=0.019c^2$). The highest yield is now about 0.108, reflecting a strong coupling strength between the two bound states.

In the fifth domain ($0.11\leq t\leq 0.12$), we lowered V_0 linearly to $1.102c^2$ (the precise value for the avoided crossing) and then kept everything constant ($0.12\leq t\leq 0.15$). In this sixth time domain, the coupling strength between the two bound states is so large that N(t) oscillates with a large period and leads to a maximum yield of 0.936. This is a rather unusual and counter-intuitive situation where the actual *decrease* of the external force strength can actually lead to an *increase* of the total pair creation yield.

It turns out that by an appropriate timing of the moments in time when the potential height is changed, we can actually maximize the yield and therefore avoid the annihilation. We have made two subsequent simulations, both of which involve changing V_0 from 1.102 to $1.092c^2$. In the first simulation the change took place between from t=0.140 to 0.142 (dotted curve) while in the second simulation we have delayed this change a little bit and reduced V_0 from t=0.150 to 0.152 (leading to the solid curve). The resulting yields monitored in the last time domain are rather different. While the earlier decrease of V_0 enhanced the yield even more, the second case decreased it first. In both situations we observe oscillations with the same period. When V_0 is $1.092c^2$, the curve oscillates with an amplitude of 0.05 around 0.98. For the second case, N(t) oscillates with an amplitude 0.13 around only 0.8. Note that the period of 0.016 in both cases is dictated by the (same) energy spacing. This example shows us that the pair creation yield can be controlled by an appropriate timing of the external field.

5. Combination of several avoided crossings

So far we have focused our attention only on the first avoided crossing. Next we will investigate a rather interesting phenomenon that occurs if more than one crossing is dynamically relevant. Below we will examine the case where the V_0 is chosen initially such that the spectrum is in the region of the first avoided crossing and then (after a delay time T) the potential strength V_0 is increased to the region of two avoided crossings. Figure 9 gives a zoomed-in view (similarly to Fig. 2) of the energy spectra of the corresponding four states. As four levels are possibly involved in the dynamics we need to extend the two-level model developed so far. The extension is summarized in Appendix C. In this extension we have ignored the coupling between the top two-level system labeled $|III\rangle$ and $|IV\rangle$ and the bottom one labeled $|V\rangle$ and $|VI\rangle$ at the second and third avoided

crossings. During the time at the first avoided crossing the states have evolved such that different initial conditions characterize the two two-level systems. This may result in the excitation of only a single instantaneous energy state and can therefore lead to the absence of any oscillations in N(t).

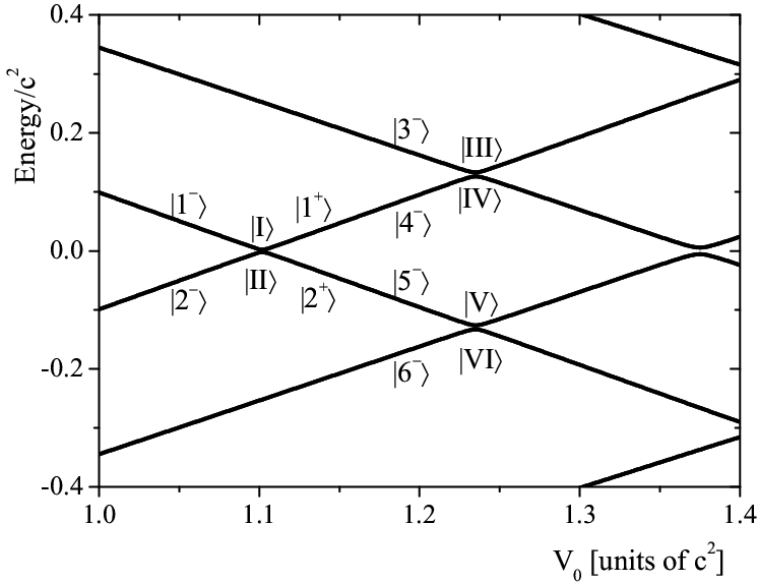

Figure 9 The energy spectrum as a function of V_0. The +(–) labels indicate bound states directly before (after) the avoided crossings. [Parameters are F=2.4/c, W=0.3/c, D=6/c.]

In Figure 9 we have drawn the energy level around the single and two crossings. We label the instantaneous states at the crossings as $|\mathrm{I}\rangle$, $|\mathrm{II}\rangle$, $|\mathrm{III}\rangle$, $|\mathrm{IV}\rangle$, $|\mathrm{V}\rangle$ and $|\mathrm{VI}\rangle$, while the states slightly away from the avoided crossings are denoted by $|1^-\rangle$, $|2^-\rangle$, $|1^+\rangle$, $|2^+\rangle$, $|3^-\rangle$, $|4^-\rangle$, $|5^-\rangle$ and $|6^-\rangle$. Here the – or + signs in the superscript denote the state before or after the crossing, respectively. In our simulations V_0 was increased at characteristic times (t_1, t_2 and t_3) to bring the dynamics to the different spectral regions. Before the first crossing, the (electronic) state $|1^-\rangle$ was initially empty while the (positronic) state $|2^-\rangle$ was occupied. This initial excitation is due to the overlap with the fully occupied states of the (force-free) negative energy continuum. When we increase V_0 at time t_1 rather abruptly towards the first crossing point, both states $|\mathrm{I}\rangle$ and $|\mathrm{II}\rangle$ become excited and as a result the particle number oscillates between 0 and 1. At time t_2 we increase V_0 further into the regime characterized by two crossings. After time t_3 the system is again in the domain of a single avoided crossing.

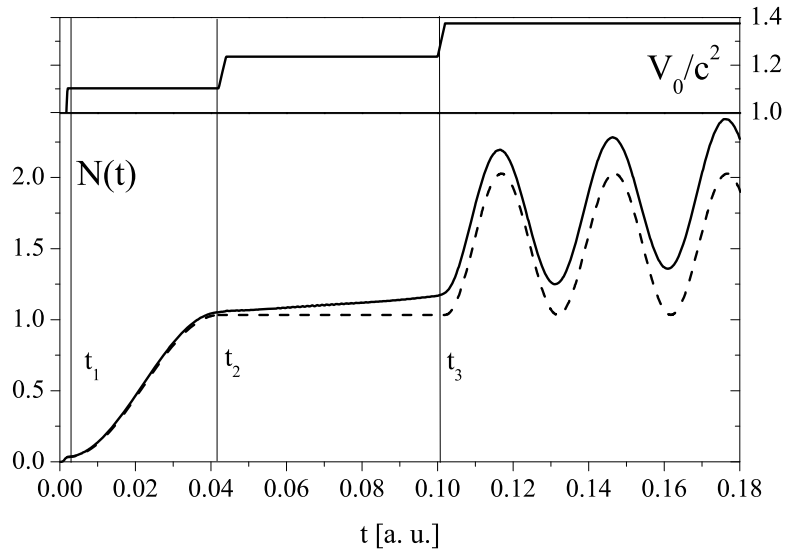

Figure 10 The yield N(t) as function of time as V_0 is increased to the three values $1.102c^2$, $1.235c^2$ and $1.375c^2$. The three vertical lines present the moments when V_0 was increased. The dashed curve is the prediction of the two-level approximation. [Parameters are F=2.4/c, W=0.3/c, D=6/c]

Figure 10 shows the number of the created particles as the height V_0 was increased in time. The three vertical lines denote the moments when potential was increased and naturally divide the evolution into regimes characteristic for $V_0 = 1.102c^2$, $1.235c^2$ and $1.375c^2$. Again, at very early times, we increased the height V_0 from 0 to $1.102c^2$ with an amplitude function $V_0(t) = 1.102c^2 \sin^2(\pi t/0.004)$ and moved the dynamics towards the first avoided crossing point. After $V_0 = 1.102c^2$ we keep it unchanged and at time t=0.042 we have the highest yield of 1.06. Then in the interval 0.042 to 0.044 we increased the height V_0 from 1.102 to $1.235c^2$ and kept the parameters unchanged for ($0.044 \le t \le 0.1$), which brings us to the region of two avoided crossings. Quite remarkably, in this interval the yield remains nearly constant and there is no oscillatory behavior even though $V_0 = 1.235c^2$ corresponds to the simultaneous presence of the second and third avoided crossing. Next we increase V_0 to $1.375c^2$ (forth avoided crossing). The yield oscillates again with a period of 0.03 and amplitude of 0.94.

The dashed line is obtained from the simplified discrete-level approximation as discussed in Appendix C. The most important observation is that the yield N(t) in the domain of the second and third avoid crossing is nearly constant, which suggests that in this particular case only a single instantaneous energy eigenstate is excited and therefore involved in the dynamics. However, it turns out that the time duration ($t_2 - t_1$) when the system is in the single-avoided crossing regime

determines the yield N(t) in the two-avoided crossing regime. In other words the build-up of the phases for $t<t_2$ is crucially important for the next time regime $t_2<t$.

We have illustrated this in Figure 11, which is identical to Figure 10, except that the switch time to region 2 was chosen earlier with $t_2 = 0.021$ instead of $t_2=0.042$.

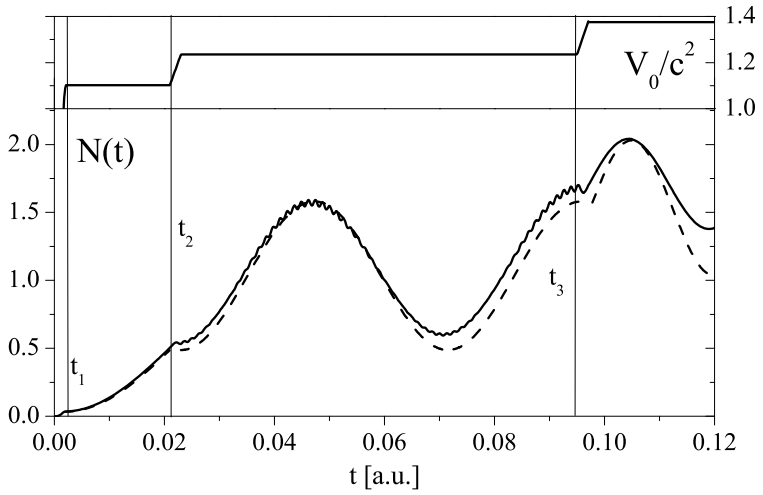

Figure 11 The yield N(t) as a function of time. The top panel presents how the height V_0 changes with time. The vertical lines present the moments when the changes take place. The dashed curve is the two-level prediction Eq. (2.3). [Parameters are F=2.4/c, W=0.3/c, D=6/c]

In this case apparently all four energy eigenstates at the two avoided crossings are excited and as a result N(t) oscillates periodically in contrast to Figure 10.

6. Summary and outlook

We have examined the pair-creation process for a static subcritical potential well next to a static potential barrier. The analysis based on numerical solutions to the Dirac equation indicates that if the separation between the well and the barrier is not too large, the discrete states from the positive and negative continuum can led to dynamically important avoided crossings. The coupling among these states can lead to the simultaneously creation of electrons subsequently trapped in the potential well and of positrons captured by the barrier. The total particle yield N(t) can exhibit a periodic oscillatory behavior where the period can be directly related to the energy gap of the corresponding two bound states. The highest yield is proportional to the total number of avoided crossings. For the interesting case where the height of the potential is increased stepwise in time, the dynamics depends crucially on the (time-dependent) phases of the states at the avoided

crossings. It is therefore (at least in principal) possible to control the pair creation yield (from oscillatory to constant in time) by an appropriate timing of the external force.

The usual pair creation process based on a single (supercritical) well depends on the so-called diving of the lowest lying electronic bound state into the negative energy continuum [17,18]. In this case numerical studies based on (quasi) – continuum states [28] reveal that the path of the discrete energy level through the negative energy continuum is also characterized by consecutive sequences of avoided crossings. However, in the true continuum limit we have unavoidably a true energy degeneracy between the discrete and continuum states. If in this case the height of the potential was turned off adiabatically back to zero, the number of created electron-positron pairs would not return back to zero, as the corresponding positron had enough time to escape to infinity and would not be able to annihilate the trapped electron in the well region. This (even adiabatically) irreversible pair creation behavior is conceptually different from our (sub-critical) dynamics, where both created particles remain trapped and therefore a truly adiabatic turn-off of the well and barrier could annihilate the pair completely.

To the best of our knowledge, this is the first time that the pair creation process is predicted for a dynamics where both the created electron and the positron are captured by the external force field. As a result only discrete states play a role and it is therefore possibly to model the pair creation process (as predicted by the Dirac equation) surprisingly accurately with a conceptually much easier phenomenological two-level model. It turns out that all basic features can be predicted if we only use the minimum energy gap and the coupling strength as free parameters in this model (that are obtained from the full Dirac solution).

In closing, we point out that while our combined well-barrier system is obviously an oversimplified and ideal theoretical model system to study the effect of discrete-discrete state interactions on the pair creation process, it is very difficult to find a concrete static realization for a direct experimental test. However, with appropriately time and spaced time-dependent external force fields that can periodically reverse the force direction one could possibly engineer related field configurations with similar properties.

Acknowledgements

We enjoyed several helpful discussions with Drs. Y.J. Li, X. Lu, Z.M. Sheng and J. Zhang.

This work has been supported by the NSF and by the National Basic Research (973) Program of China (#2013CBA01501, #2013CBA01504) and NSFC (#11135012).

Appendix A The numerical method to solve the Dirac equation

To study the electron-positron creation process, the single-particle quantum mechanical description is not sufficient and quantum field theory is necessary. The particle creation and annihilation are described by the field operator that satisfies the time-dependent Heisenberg as well as the Dirac equation [18]:

$$i\partial\,\hat{\psi}(x,t)/\partial t = [c\sigma_1 p_x + \sigma_3 c^2 + V(x,t)]\,\hat{\psi}(x,t) \qquad (A.1)$$

In our model system the external force is represented by a scalar potential V(x) that varies only in the x-direction. If we focus on a single spin, the usual four-component spinor wave function can be reduced to only two components, $\psi(x,t)=\begin{pmatrix}\varphi_1\\ \varphi_2\end{pmatrix}$, and the Dirac matrices reduce to the usual Pauli matrices σ_i, with i=1, 2, 3. We adopt atomic units from now on where the speed of light is c=137.036 a.u.. The field operator may be expanded using time independent or time evolved energy eigen-functions of the field-free Dirac equation as [29]:

$$\begin{aligned}\hat{\psi}(x,t)&=\sum_p \hat{b}_p(t)W_p(x)+\sum_p \hat{d}_n^{\dagger}(t)W_n(x)\\ &=\sum_p \hat{b}_p(t=0)W_p(x,t)+\sum_n \hat{d}_n^{\dagger}(t=0)W_n(x,t)\end{aligned} \qquad (A.2)$$

Here $W_p(x)$ and $W_n(x)$ represent the field-free energy eigenstates $|p\rangle$ and $|n\rangle$ in the spatial representation at t=0. Note that $W_p(x,t)$ and $W_n(x,t)$ satisfy the single-particle time-dependent Dirac equation Eq. (A1). From Eq. (A2), we obtain

$$\hat{b}_p(t)=\sum_{p'} \hat{b}_{p'}(t=0)\langle p|U(t)|p'\rangle+\sum_{n'} \hat{d}_{n'}^{\dagger}(t=0)\langle p|U(t)|n'\rangle \qquad (A.3a)$$

$$\hat{d}_n^{\dagger}(t)=\sum_{p'} \hat{b}_{p'}(t=0)\langle n|U(t)|p'\rangle+\sum_{n'} \hat{d}_{n'}^{\dagger}(t=0)\langle n|U(t)|n'\rangle \qquad (A.3b)$$

where the coefficients are the matrix elements of the time-ordered propagator $U(t)=\exp\{-i\int^t dt'\,[c\sigma_1 p+\sigma_3 c^2+V(x,t')]\}$ between the energy eigenstates.

The electrons' spatial probability density can be obtained from the expectation value of the

product of the electronic field operators:

$$\rho(x,t) = \langle\langle vac \| \hat{\psi}_e^{\dagger}(x,t)\hat{\psi}_e(x,t) \| vac\rangle\rangle \tag{A.4}$$

which can be considered as the electron probability density, here $\hat{\psi}_e(x,t) \equiv \sum_p b_p(t)W_p(x)$ is the electronic portion of the field operator. After some operator algebra and using the commutator relations $\left[\hat{b}_p, \hat{b}_{p'}^{\dagger}\right]_+ = \hat{b}_p\hat{b}_{p'}^{\dagger} + \hat{b}_{p'}^{\dagger}\hat{b}_p = \delta_{p,p'}$ and $\left[\hat{d}_n, \hat{d}_{n'}^{\dagger}\right]_+ = \delta_{n,n'}$ the density can be expressed through the field-free energy eigenstates of the single-particle Hamiltonian as:

$$\rho(x,t) = \sum_n \left| \sum_p U_{p,n}(t)W_p(x) \right|^2 \tag{A.5}$$

where $U_{p,n}(t) = \langle p | n(t)\rangle = \langle p | U(t) | n\rangle$. By integrating this equation over space, we obtain the total number of the created pairs as

$$N(t) = \int dx\, \rho(x,t) = \sum_{p,n} \left| U_{p,n}(t) \right|^2 \tag{A.6}$$

In order to compute the matrix elements $U_{pn}(t)$, we use the split operator numerical technique [30-33] to evolve each state $|n\rangle$ in time to get $|n(t)\rangle$ followed by the projection onto the states $|p\rangle$. In contrast to the usual S-matrix method, this method can predict the creation behavior at any time and space.

Appendix B Instantaneous eigenstates and dynamics of the two-state approach

In dynamical regions where neither the amplitude V_0 nor the spacing F varies too rapidly in time, the instantaneous energy eigenvectors and eigen energies of the effective two-state Hamiltonian are relevant. At any instant of time t, the matrix H has a positive and negative eigenvalue determined by the eigenvalue equation:

$$[\, c\, \sigma_1\, p_x + \sigma_3\, c^2 + V(x,t)\,]\, \chi(x) = E\, \chi(x) \tag{B.1}$$

$$E_{pos} = [(c^2\text{-}v)^2 + \lambda^2]^{1/2} \tag{B.2a}$$

$$E_{neg} = -[(c^2-v)^2+\lambda^2]^{1/2} \quad \text{(B.2b)}$$

and the corresponding eigenvectors

$$V_{pos} = \{V_{pos1}, V_{pos2}\} = N_{pos}\{c^2-v+E_{pos}, \lambda\} \quad \text{(B.3a)}$$

$$V_{neg} = \{V_{neg1}, V_{neg2}\} = N_{neg}\{c^2-v-E_{pos}, \lambda\} \quad \text{(B.3b)}$$

where N_{pos} and N_{neg} denote the normalization factors. We have shown above that as v is increased from 0 to $2c^2$ [for the special case of no coupling (λ=0)] the eigenvector remains {0,1} [denoted as V_{neg} for $v<c^2$] and {1,0} [denoted as V_{pos} for $v>c^2$]. On the other hand, as v grows from 0 to $2c^2$, the electronic state remains {1,0} while its eigenvalue is lowered from c^2 to $-c^2$.

For $\lambda \neq 0$, however, and in the vicinity of the crossing ($v=c^2$) the eigenvalues are $E_{pos} = \lambda$ and $E_{neg} = -\lambda$, while the eigenvectors are $V_{pos} = \{1, 1\}/\sqrt{2}$ and $V_{neg} = \{-1,1\}\sqrt{2}$. This behavior is summarized in Fig. A.1, showing that this eigen state with negative energy changes from {0,1} to {1,0}. In other words, it changes its character entirely from a positronic to an electronic state.

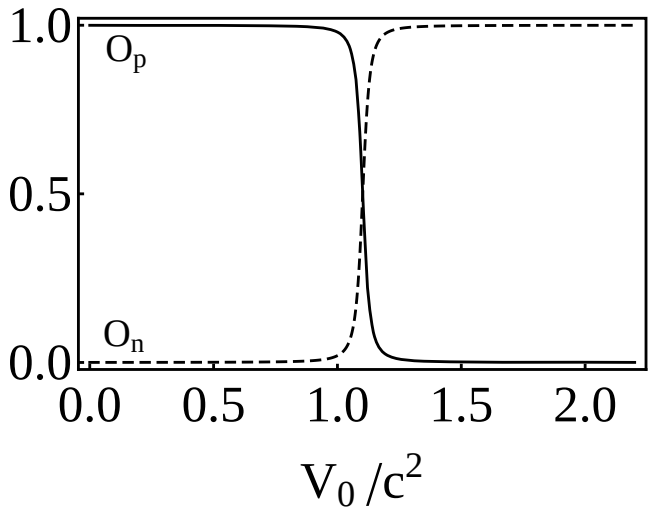

Figure A1 The amplitudes $\{O_p, O_n\}$ of the instantaneous (negative) energy eigenvector of the effective two-state Hamiltonian as a function of the potential V_0.

It turns out that the instantaneous eigenvectors can play an important role for both abruptly as well as adiabatically turned on force fields. If the external force field was turned on very slowly

(adiabatically) all initially occupied states $|\square\rangle$ would maintain their occupation but become the instantaneous eigenvectors. This means that the positronic state analyzed above remains fully excited. However, our definition of the particle yield corresponds to the actual particle number we would observe, if the potential was turned off abruptly. Consistent with this definition we obtain $N = O_n(E_{neg}) \equiv \Sigma_n |\langle E_{neg}|n\rangle|^2$. Figure A.1 therefore suggests that if v changes very slowly (adiabatically) from v=0 to $v=2c^2$ (and the state remains in the lower energetic instantaneous eigenstate V_{neg}) according to this simplified model the total number of pairs (given by $N(t)=|V_{neg1}|^2$) should change monotonically from N(t)=0 (for v=0) to N(t)=0.5 (for $v=1.102c^2$) to finally N(t)=1 (for $v=2c^2$).

$$N(t) = |V_{neg1}|^2 = \{ c^2\text{-}v\text{-}E_{pos} \}^2 / [\{ c^2\text{-}v\text{-}E_{pos} \}^2 + \lambda^2] \qquad (B.4)$$

If, on the other hand, the external field V(x) is turned on rather abruptly to the avoided crossing, then the initially occupied negative energy eigenstates would instantly populate the two eigenstates V_{pos} and V_{neg} with an amplitude given by the overlap scalar product $\langle\{0,1\}|V_{pos}\rangle = V_{pos2}$ and $\langle\{0,1\}|V_{neg}\rangle = V_{neg2}$. The time evolution of the state afterwards is then given by

$$|\Psi(t)\rangle = \exp(-i\, E_{pos} t)\, V_{pos2}|V_{pos}\rangle + \exp(-i\, E_{neg} t)\, V_{neg2}|V_{neg}\rangle \qquad (B.5)$$

The associated number of created particles defined as $N(t) = |\langle(1,0)|\Psi(t)\rangle|^2$ would be

$$N(t) = |\exp(-i\, E_{pos}\, t)\, V_{pos2}V_{pos1} + \exp(-i\, E_{neg} t)\, V_{neg2}V_{neg1}|^{\square} \qquad (B.6)$$

This describes an oscillatory behavior with a period $T=2\pi/(E_{pos}-E_{neg})$ and a maximum value given by

$$N_{max} = V_{pos1}{}^2\, V_{pos2}{}^2 + V_{neg1}{}^2\, V_{neg2}{}^2 + 2\,|V_{pos1}V_{pos2}V_{neg1}V_{neg2}| \qquad (B.7)$$

Note that in this model, we always have N(t=0)=0, as the initial state was assumed to be the vacuum

and it requires a time $\pi/(E_{pos} - E_{neg})$ for the electron-positron pair to be created. In other words, if the sudden turn-on of v was immediately followed by a sudden turn-off, we would not find any created particles. Furthermore, if the abrupt turn-off would happen after an integer multiples of the period T, we would also not find any permanently created pairs. This periodic creation and annihilation of pairs is an interesting coherence effect.

Appendix C The extension of the two-level model to multiple avoided crossings

In order to better understand what happens at multiple avoided crossings, we start our discussion with a summary of the case of a single avoided crossing. The number of created electrons is defined from the time evolution of the (force-free) negative energy continuum state as

$$N(t) = \Sigma_{n,p} |\langle p|n(t)\rangle|^2 \qquad (C.1)$$

Due to the relatively quick turn-on of the potential to the region of the first avoided crossing, we can expand each initial state $|n\rangle$ in the energy eigenbasis given by the bound states $|I\rangle$ and $|II\rangle$ and the other remaining instantaneous eigenstates $|P\rangle$, $|N\rangle$ (associated with the positive and negative energy continua) as

$$|n\rangle = \Sigma_P |P\rangle\langle P|n\rangle + \Sigma_N |N\rangle\langle N|n\rangle + |I\rangle\langle I|n\rangle + |II\rangle\langle II|n\rangle \qquad (C.2)$$

As each initial state $|n\rangle$ is from the negative (field-free) energy continuum its overlap with the (dressed) positive energy state $\langle P|n\rangle$ is negligible compared to other contributions in Eq. (C.2). The time evolution of the state $|n\rangle$ can therefore be approximated as

$$|n(t)\rangle = \exp(-i E_I t)|I\rangle \langle I|n\rangle + \exp(-i E_{II} t) |II\rangle \langle II|n\rangle + \Sigma_N \exp(-i E_N t) |N\rangle \langle N|n\rangle \qquad (C.3)$$

As a result the projection of $|n(t)\rangle$ onto the (field free) positive energy state $|p\rangle$ required in the determination of N(t) is

$$\langle p|n(t)\rangle = \exp(-i E_I t) \langle p|I\rangle \langle I|n\rangle + \exp(-i E_{II} t) \langle p|II\rangle \langle II|n\rangle + \Sigma_N \exp(-i E_N t) \langle p|N\rangle \langle N|n\rangle \qquad (C.4)$$

Using a similar reasoning as above, also the overlap between $|p\rangle$ and $|N\rangle$ is very small such that we can further approximate $\langle p|n(t)\rangle = \exp(-i\, E_I\, t)\, \langle p|I\rangle\langle I|n\rangle + \exp(-i\, E_{II}\, t)\, \langle p|II\rangle\langle II|n\rangle$. With this expression the time-dependence of the particle number N(t) in the region of a single avoided crossing can be expressed as

$$N(t) = \Sigma_{n,p} \left[\langle p|I\rangle\langle I|n\rangle\langle n|I\rangle\langle I|p\rangle + \langle p|II\rangle\langle II|n\rangle\langle n|II\rangle\langle II|p\rangle + \right.$$
$$\left. + \exp(-i\, \Delta E\, t)\, \langle p|I\rangle\langle I|n\rangle\langle n|II\rangle\langle II|p\rangle + \exp(i\, \Delta E\, t)\, \langle p|II\rangle\langle II|n\rangle\langle n|I\rangle\langle I|p\rangle\right] \qquad (C.5)$$

where $\Delta E \equiv E_I - E_{II}$. Note that $\Sigma_{n,p} \left[\langle p|I\rangle\langle I|n\rangle\langle n|I\rangle\langle I|p\rangle + \langle p|II\rangle\langle II|n\rangle\langle n|II\rangle\langle II|p\rangle\right]$ is constant while $\Sigma_{n,p}$ $\left[\exp(-i\, \Delta E\, t)\, \langle p|I\rangle\langle I|n\rangle\langle n|II\rangle\langle II|p\rangle + \exp(i\, \Delta E\, t)\, \langle p|II\rangle\langle II|n\rangle\langle n|I\rangle\langle I|p\rangle\right]$ oscillates in time. If we abbreviate the positive and negative energy subspace projection operators as $P_+ \equiv \Sigma_p\, |p\rangle\langle p|$ and $P_- \equiv \Sigma_n\, |n\rangle\langle n|$, the expression for the yield N(t) simplifies to

$$N(t) = \langle I|P_-|I\rangle\langle I|P_+|I\rangle + \langle II|P_-|II\rangle\langle II|P_+|II\rangle +$$
$$+ \exp(-i\, \Delta E\, t)\, \langle I|P_-|II\rangle\langle II|P_+|I\rangle + \exp(i\, \Delta E\, t)\, \langle II|P_-|I\rangle\langle I|P_+|II\rangle \qquad (C.6)$$

In order to make contact with our instantaneous eigenvectors of the effective two-level theory we use $P_- = \{0,1\} \otimes \{0,1\}^T$ and similarly $P_+ = \{1,0\} \otimes \{1,0\}^T$, where the T denotes the transposed vector. Also, the instantaneous bound states can be expressed as $|I\rangle = \{1,1\}/\sqrt{2}$ and $|II\rangle = \{-1,1\}/\sqrt{2}$. According to these simplifications, we obtain the particle number as shown by the dashed line in Fig. 5, which oscillates between the values of 0 and 1.

Next we examine the more complicated situation where after a characteristic time T (which is spent at the first avoided crossing) the potential V_0 is increased to enter the region where we have two avoided crossings. Here we denote the bound states in the energy gap at the second and third avoided crossing points by $|III\rangle$, $|IV\rangle$, $|V\rangle$ and $|VI\rangle$ from top to bottom according to their energy value as shown in Fig. 9. As these states are complicated superposition states of the (force-free) positive and negative energy manifold, it is advantageous to also introduce the states just before the avoided crossings, as these are either electronic or positronic. These are denoted by $|3^-\rangle$, $|4^-\rangle$, $|5^-\rangle$ and $|6^-\rangle$ in Figure 9. For example, for V_0 slightly before the avoided crossing $|1^-\rangle$ is an electronic

state and $|2^-\rangle$ is a positronic state, while just after the avoided crossing $|1^+\rangle$ reverses its nature and becomes positronic while $|2^+\rangle$ becomes electronic as suggested in Fig. A.1. Expressed in these states, the state $|n(T)\rangle$ of the system at time T is

$$\begin{aligned}|n(T)\rangle = & \exp(-i E_I T)|1^+\rangle \langle 1^+|n\rangle + \exp(-i E_{II} T) |2^+\rangle \langle 2^+|n\rangle + \Sigma_N \exp(-i E_N T) |N\rangle \langle N|n\rangle \\ & \equiv C_{I,n}(T) |1^+\rangle + C_{II,n}(T) |2^+\rangle + \Sigma_N C_{N,n}(T) |N\rangle \end{aligned} \quad (C.7)$$

While the terms $\Sigma_N C_{N,n}(T) |N\rangle$ do not contribute the total particle yield N(t), they are crucially important with regard to the excitation of the eigenstates at the double avoided crossings for larger V_0. We can also decompose this state $|n(T)\rangle$ in terms of the instantaneous eigenstates, just before the second and third avoided crossing points:

$$\begin{aligned}|n(T)\rangle = & \Sigma_{P'} |P'\rangle\langle P'|n(T)\rangle + \Sigma_{N'} |N'\rangle\langle N'|n(T)\rangle + |3^-\rangle\langle 3^-|n(T)\rangle \\ & + |4^-\rangle\langle 4^-|n(T)\rangle + |5^-\rangle\langle 5^-|n(T)\rangle + |6^-\rangle\langle 6^-|n(T)\rangle \end{aligned} \quad (C.8)$$

As $|n(T)\rangle$ is essentially a positronic state it has only a small overlap with the positive continuum states $|P'\rangle$ and we can ignore the first term in the expansion. When we make the inner product with the positive field free state $|p\rangle$ to predict the creation yield, the second term in the expression is also negligible as $\langle p|N'\rangle << 1$. This means we can approximate $|n(T)\rangle$ as

$$|n(T)\rangle = |3^-\rangle\langle 3^-|n(T)\rangle + |4^-\rangle\langle 4^-|n(T)\rangle + |5^-\rangle\langle 5^-|n(T)\rangle + |6^-\rangle\langle 6^-|n(T)\rangle \quad (C.9)$$

We note that $|3^-\rangle$ and $|5^-\rangle$ are electronic states while $|4^-\rangle$ and $|6^-\rangle$ are positronic. Moreover, $|3^-\rangle$ and $|6^-\rangle$ are the first excited states of the electron and positron, respectively, while $|4^-\rangle$ and $|5^-\rangle$ are the ground states. If we insert the approximate expression for $|n(T)\rangle$ from Eq. (C.7) into the right hand-side of Eq. (C.9) we obtain the 12 terms

$$\begin{aligned}|n(T)\rangle = & C_{I,n}(T) |3^-\rangle\langle 3^-|1^+\rangle + C_{II,n}(T) |3^-\rangle\langle 3^-|2^+\rangle + \Sigma_N C_{N,n}(T) |3^-\rangle\langle 3^-|N\rangle + \\ & + C_{I,n}(T) |4^-\rangle\langle 4^-|1^+\rangle + C_{II,n}(T) |4^-\rangle\langle 4^-|2^+\rangle + \Sigma_N C_{N,n}(T) |4^-\rangle\langle 4^-|N\rangle + \end{aligned}$$

$$+ C_{I,n}(T)\,|5^-\rangle\langle 5^-|1^+\rangle + C_{II,n}(T)\,|5^-\rangle\langle 5^-|2^+\rangle + \Sigma_N\, C_{N,n}(T)\,|5^-\rangle\langle 5^-|N\rangle +$$
$$+ C_{I,n}(T)\,|6^-\rangle\langle 6^-|1^+\rangle + C_{II,n}(T)\,|6^-\rangle\langle 6^-|2^+\rangle + \Sigma_N\, C_{N,n}(T)\,|6^-\rangle\langle 6^-|N\rangle \qquad \text{(C.10)}$$

Fortunately several of these overlap matrix elements are rather small compared to others and can be omitted. For example we can assume that any overlap of states of the positronic with those of the electronic manifold is small,

$$\langle 3^-|1^+\rangle \approx 0, \quad \langle 3^-|2^+\rangle \approx 0, \quad \Sigma_N\, C_{N,n}(T)\,\langle 3^-|N\rangle \approx 0$$
$$\langle 4^-|1^+\rangle \approx 1, \quad \langle 4^-|2^+\rangle \approx 0, \quad \Sigma_N\, C_{N,n}(T)\,\langle 4^-|N\rangle \approx 0$$
$$\langle 5^-|1^+\rangle \approx 0, \quad \langle 5^-|2^+\rangle \approx 1, \quad \Sigma_N\, C_{N,n}(T)\,\langle 5^-|N\rangle \approx 0$$
$$\langle 6^-|1^+\rangle \approx 0, \quad \langle 6^-|2^+\rangle \approx 0, \quad \Sigma_N\, C_{N,n}(T)\,\langle 6^-|N\rangle \approx C_{s,n}(T) \qquad \text{(C.11)}$$

As a result, the state $|n(T)\rangle$ in (C.10) can be significantly simplified to:

$$|n(T)\rangle \approx C_{I,n}(T)\,|4^-\rangle + C_{II,n}(T)\,|5^-\rangle + C_{s,n}(T)\,|6^-\rangle \qquad \text{(C.12)}$$

The states $|4^-\rangle$, $|5^-\rangle$ and $|6^-\rangle$ can be expressed in terms of the eigen states at the avoided crossing as $|4^-\rangle = (|III\rangle + |IV\rangle)/\sqrt{2}$, $|5^-\rangle = (|V\rangle - |VI\rangle)/\sqrt{2}$ and $|6^-\rangle = (|V\rangle + |VI\rangle)/\sqrt{2}$. If we replace the states with those states exactly at the avoided crossing, the state $|n(T)\rangle$ can be written as

$$|n(T)\rangle \approx C_{I,n}(T)\,(\,|III\rangle + |IV\rangle\,)/\sqrt{2} +$$
$$+ (\,C_{II,n}(T) + C_{s,n}(T)\,)/\sqrt{2}\,|V\rangle + (C_{s,n}(T) - C_{II,n}(T)\,)/\sqrt{2}\,|VI\rangle \qquad \text{(C.13)}$$

After these numerous projections, we finally evolve the state $|n(T)\rangle$ further in time for a new potential strength V_0 for which the states $|III\rangle$, $|IV\rangle$, $|V\rangle$ and $|VI\rangle$ are energy eigenstates. For $t>T$ we obtain

$$|n(t)\rangle = \exp(-i\,E_{III}\,(t-T))\,C_{I,n}(T)/\sqrt{2}\,|III\rangle + \exp(-i\,E_{IV}\,(t-T))\,C_{I,n}(T)/\sqrt{2}\,|IV\rangle +$$
$$+ \exp(-i\,E_V\,(t-T))\,(\,C_{II,n}(T) + C_{s,n}(T)\,)/\sqrt{2}\,|V\rangle$$
$$+ \exp(-i\,E_{VI}\,(t-T))\,(C_{s,n}(T) - C_{II,n}(T)\,)/\sqrt{2}\,|VI\rangle \qquad \text{(C.14)}$$

We note that the second and third avoided crossings are decoupled from each other and have a similar spinor structure, such that we can treat them separately. Thus we can approximate the state $|n(t)\rangle$ by

$$\begin{aligned}|n(t)\rangle \approx & \{\exp(-i\, E_{III}\,(t-T)\, C_{I,n}(T) + \exp(-i\, E_V\,(t-T))\,(\, C_{II,n}\,(T) + C_{s,n}(T)\,)\}/\sqrt{2}\,|III\rangle \\ & + \{\exp(-i\, E_{IV}\,(t-T))\, C_{I,n}(T) \;+ \exp(-i\, E_{VI}\,(t-T))\,(\, C_{s,n}(T) - C_{II,n}\,(T)\,)\}/\sqrt{2}\,|IV\rangle \\ & \equiv \Lambda_{+,n}(t)\,|III\rangle + \Lambda_{-,n}(t)\,|IV\rangle \end{aligned} \qquad \text{(C.15)}$$

We note that due to the structure of the coefficients $C_{s,n}(T)$ and $C_{II,n}\,(T)$, it is possible to find some characteristic time T for which the co-factor $\Lambda_{-,n}(t)$ vanishes identically for all times $t>T$. In other words, only the single state $|III\rangle$ might be excited then. The particle number N(t) can be obtained by projecting the states $|n(t)\rangle$ onto $|p\rangle$ and we obtain the final result

$$\begin{aligned}N(t) = & \Sigma_n\,[|\Lambda_{+,n}(t)|^2\,\langle III|\,P_+|III\rangle + |\Lambda_{-,n}(t)|^2\,\langle IV|\,P_+|IV\rangle] + \\ & + \Sigma_n\,[\Lambda_{+,n}(t)\Lambda_{-,n}(t)^*\,\langle IV|\,P_+|III\rangle + \Lambda_{-,n}(t)\Lambda_{+,n}(t)^*\,\langle III|\,P_+|IV\rangle] \end{aligned} \qquad \text{(C.16)}$$

This expression suggests that the evolution of N(t) for $t>T$ depends crucially on the coefficients $C_{I,n}(T)$ and $C_{s,n}(T) - C_{II,n}\,(T)$.

References

[1] F. Sauter, Z. Phys. 69, 742 (1931).

[2] W. Heisenberg and H. Euler, Z. Phys. 98, 714 (1936).

[3] J.S. Schwinger, Phys. Rev. 82, 664 (1951).

[4] For a recent review, see A. Di Piazza, C. Müller, K.Z. Hatsagortsyan and C.H. Keitel, Rev. Mod. Phys. 84, 1177 (2012).

[5] A. Hansen and F. Ravndal, Phys. Scr. 23, 1036 (1981).

[6] B.R. Holstein, Am. J. Phys. 66, 507 (1998); Am. J. Phys. 67, 499 (1999).

[7] R. Schützhold, H. Gies and G. Dunne, Phys. Rev. Lett. 101, 130404 (2008).

[8] M. Ruf, G.R. Mocken, C. Müller, K.Z. Hatsagortsyan and C.H. Keitel, Phys. Rev. Lett. 102, 080402 (2009).

[9] T. Cheng, Q. Su and R. Grobe, Phys. Rev. A 80, 013410 (2009).

[10] S.S. Bulanov, V.D. Mur, N.B. Narozhny, J. Nees and V.S. Popov, Phys. Rev. Lett. 104, 220404 (2010).

[11] R.G. Newton, Phys. Rev. 96, 523 (1954).

[12] W.Y. Tsai and A. Yildiz, Phys. Rev. D 8, 3446 (1973).

[13] V.N. Baier, V.M. Katkov and V.M. Strakhovenko, Sov. Phys. JETP 40, 225 (1974).

[14] S.P. Kim and D.N. Page, Phys. Rev. D 65, 105002 (2002); Phys. Rev. D 75, 045013 (2007).

[15] G.V. Dunne and C. Schubert, Phys. Rev. D 72, 105004 (2005); Phys. Rev. D 73, 065028 (2006).

[16] R. Schützhold, H. Gies and G. Dunne, Phys. Rev. Lett. 101, 130404 (2008).

[17] B. Müller, H. Peitz, J. Rafelski and W. Greiner, Phys. Rev. Lett. 28, 1235 (1972).

[18] For a review, see, e.g., W. Greiner, B. Müller and J. Rafelski, "Quantum Electrodynamics of Strong Fields" (Springer Verlag, Berlin, 1985).

[19] M. Jiang, Q.Z. Lv, Z.M. Sheng, R. Grobe and Q. Su, Phys. Rev. A 87, 042503 (2013).

[20] P. Krekora, Q. Su and R. Grobe, Phys. Rev. A 73, 022114 (2006).

[21] F. Fillion-Gourdeau, E. Lorin and A.D. Bandrauk, Phys. Rev. Lett. 110, 013002 (2013).

[22] S. Tang, B. Xie, D. Lu, H. Wang, L. Fu and J. Liu, Phys. Rev. A 88, 012106 (2013).

[23] W.P. Reinhardt, Ann. Rev. Phys. Chem. 33, 223 (1982).

[24] N. Moiseyev, Phys. Rep. 302, 211 (1998).

[25] For an application to relativistic systems, see A.D. Alhaidari, Phys. Rev. A 75, 042707 (2007).

[26] Q.Z. Lv, Y. Liu, Y.J. Li, R. Grobe and Q. Su, Phys. Rev. Lett.111, 183204 (2013).

[27] P. Krekora, K. Cooley, Q. Su and R. Grobe, Phys. Rev. Lett. 95, 070403 (2005).

[28] For review, see T. Cheng, Q. Su and R. Grobe, Contemp. Phys. 51, 315 (2010).

[29] A.D. Bandrauk and H. Shen, J. Phys. A 27, 7147 (1994).

[30] J.W. Braun, Q. Su, and R. Grobe, Phys. Rev. A 59, 604 (1999).

[31] G.R. Mocken and C.H. Keitel, Comp. Phys. Commun. 178, 868 (2008).

[32] M. Ruf, H. Bauke, and C.H. Keitel, J. Comp. Phys. 228, 9092 (2009).

[33] For an exception, see, C.C. Gerry, Q. Su and R. Grobe, Phys. Rev. A 74, 044103 (2006).